Computers and Concrete, *Vol. 25, No. 6 (2020) 551-563*
DOI: https://doi.org/10.12989/cac.2020.25.6.551

Artificial neural network calculations for a receding contact problem

Ecren Uzun Yaylacı*[1], Murat Yaylacı[2a], Hasan Ölmez[3b] and Ahmet Birinci[4c]

[1]*Department of Fisheries Technology Engineering, Karadeniz Technical University, Trabzon, Turkey*
[2]*Department of Civil Engineering, Recep Tayyip Erdogan University, Rize, Turkey*
[3]*Department of Marine Engineering Operations, Karadeniz Technical University, Trabzon, Turkey*
[4]*Department of Civil Engineering, Karadeniz Technical University, Trabzon, Turkey*

(*Received March 12, 2020, Revised May 18, 2020, Accepted May 24, 2020*)

Abstract. This paper investigates the artificial neural network (ANN) to predict the dimensionless parameters for the maximum contact pressures and contact areas of a contact problem. Firstly, the problem is formulated and solved theoretically by using Theory of Elasticity and Integral Transform Technique. Secondly, the contact problem has been extended based on the ANN. The multilayer perceptron (MLP) with three-layer was used to calculate the contact distances. External load, distance between the two quarter planes, layer heights and material properties were created by giving examples of different values were used at the training and test stages of ANN. Program code was rewritten in C++. Different types of network structures were used in the training process. The accuracy of the trained neural networks for the case was tested using 173 new data which were generated via theoretical solutions so as to determine the best network model. As a result, minimum deviation value (difference between theoretical and C++ ANN results) of was obtained for the network model. Theoretical results were compared with artificial neural network results and well agreements between them were achieved.

Keywords: contact problem; artificial neural network; quarter plane; multilayer perceptron; theory of elasticity

1. Introduction

An artificial neural network is a very useful and effective computational module of information processing models. Recently, it is used to estimate the result of any problem or case from physical or social sciences utilizing some input values and their relations. This can be described as a simulation of the human brain. This tool can be used for pattern recognition/classification or function approximation problems and very accurate results can be obtained. It is a very powerful tool for problems which involve even nonlinear relationship between input and output data. It analyzes the input and output data given to the network like a human brain, then forms a network which consists of a lot of relations. Adjusts these relations and finally trained neural network is utilized to estimate calculate the values of outputs. Numerical calculation methods, which produce approximate solutions with computer programs, provide quite convenience in solving engineering problems where theoretical solution can take a lot of time. As a powerful modeling tool, ANN offers many advantages over conventional statistical methods, as it can define complex and nonlinear relationships between parameters without any assumptions. With the artificial neural network method which may be an alternative to the current calculation methods, many researchers have obtained very reliable results in civil engineering and contact mechanics applications in recent years.

Neural networks have gained a broad interest in civil engineering problems. They are used as an alternative to statistical and optimization methods as well as in combination with numerical simulation systems.

Application examples in Civil Engineering are forecasting, water management, controls and decision support systems. The application of ANN is used in tidal level forecasting to accurately estimate the tidal level for the complex bottom topography in the near-shore area. It is also used to estimate the earthquake-induced liquefaction potential which is essential for the civil engineers in the design procedure. This model is further applied in evaluation of the wave-induced seabed instability particularly important for coastal geotechnical engineers involved in the design of marine structures (such as offshore platform, pipeline and caisson etc.).

One of the first studies of artificial neural network on civil engineering applications was made by Vanluchene and Sun (1990). The prediction of the compressive stresses in concrete is discussed by Ni and Wang (2000), and the prediction of the final shear force of prestressed concrete high beams is determined by Sanad and Saka (2001), and the relationship between vibration velocity and pressure resistance in concrete at various ages is discussed by Tang *et al*. (2007). Hanna (2007) in his paper proposed a general regression neural network model to assess nonlinear liquefaction potential of soil. Topcu *et al*. (2009), developed a feed forward artificial neural network model to model the corrosion currents of the reinforced concrete structure. Lin (2009) created an empirical model for assessing failure

*Corresponding author, Ph.D.
E-mail: ecrenuzun@ktu.edu.tr
[a]Associate Professor
[b]Assistant Professor
[c]Professor

ISSN: 1598-8198 (Print), 1598-818X (Online)

potential of highway slopes, with a special attention to the failure characteristics of the highway slopes in the Alishan, Taiwan area prior to, and post, the 1999 Chi-Chi, Taiwan earthquake. Dehbozorgi during his research investigated an application of Neuro-Fuzzy classifier for short-term earthquake prediction using saved seismogram data. This method is able to predict earthquakes five minute before, with an acceptable accuracy (Dehbozorgi 2010). Sipos *et al*. (2013) used sensitivity and dimensionless parameter approach to estimate the behavior of reinforced concrete frame and infill walls under in-plane load. Garzon-Roca *et al*. (2013) proposed a new artificial neural network technique to estimate the maximum vertical load capacity of the brick wall on the basis of experimental data. Calibration of linear and nonlinear parameters with Levenberg-Marquardt back-propagation ANN model was studied by Hasancebi and Dumlupinar (2013) and high accuracy was obtained.

Estimation of contact stress in composite plates was studied by Chandrashekhara *et al*. (1998), estimation of contact distances between an elastic layer and two circular punches using ANN by Ozsahin *et al*. (2004), and calculation of maximum contact stresses by Cakiroglu *et al*. (2005). In their study, Hattori and Serpa (2015), investigated the potential of artificial neural networks to estimate the value of some parameters used in the ANSYS package program for the contact problem. Keskin and Arslan (2013) developed an artificial neural network model for predicting the diagonal cracking strength of RC slender beams without stirrups. Erdem *et al*. (2013) used artificial neural networks analysis to predict the compression strength of polypropylene fibre mixed concrete. The main purpose of the study of Mohebbi *et al*. (2010) includes investigation of the rheological properties of fresh self-consolidating cement paste containing chemical and mineral additives using artificial neural network model. Lingam and Karthikeyan (2013) aimed at adapting artificial neural networks to predict the compressive strength of High-Performance Concrete (HPC) containing binary and quaternary blends.

In addition to these precious studies, here is some important recent studies about using ANN method for concrete structural analysis. Asteris *et al*. (2019) applied the artificial neural networks for the prediction of the compressive strength of cement-based mortars. Chitgar and Berenjian (2019) utilized from the Elman neural networks for predicting the mechanical properties of Self-Compacting Concretes (SCCs). Asteris *et al*. (2019) used the artificial neural networks approach to estimate the ultimate shear capacity of reinforced concrete beams with transverse reinforcement. Behforouz *et al*. (2019) aim to investigate the mechanical properties and durability of sustainable concrete containing waste ceramic powder (WCP), and to predict the results using artificial neural network in their study. Arani *et al*. (2019) presents a computational rational model to predict the ultimate and optimized load capacity of reinforced concrete (RC) beams strengthened by a combination of longitudinal and transverse fiber reinforced polymer (FRP) composite plates/sheets. Ozturk *et al*. (2018) studied the alkali activation of Electric Arc Furnace Slag (EAFS) with a comprehensive test program using artificial neural network method. Kong *et al*. (2016) studied the evaluation of the effect of aggregate on concrete permeability using grey correlation analysis and ANN. Ongpeng *et al*. (2016) focused on modeling the behavior of the compressive stress using the average strain and ultrasonic test results in concrete. They used feed forward backpropagation artificial neural network models to compare four types of concrete mixtures with varying water cement ratio (WC), ordinary concrete (ORC) and concrete with short steel fiber reinforcement (FRC). Camões and Martins (2016) studied about compressive strength prediction of CFRP confined concrete using data mining techniques. Saha *et al*. (2017) used artificial neural network to predict the compressive strength of self-compacting concrete in their study. Gazder *et al*. (2017) studied the predicting compressive strength of blended cement concrete with ANNs. Ashteyat and Ismeik (2017) studied predicting residual compressive strength of self-compacted concrete under various temperatures and relative humidity conditions by artificial neural networks. Hodhod *et al*. (2018) studied about prediction of creep in concrete using genetic programming hybridized with ANN. Shirkhani *et al*. (2019) studied about prediction of bond strength between concrete and rebar under corrosion using artificial neural network.

There are also important studies about structural contact mechanics including tribology and wear using artificial neural network method. Shebani and Iwnicki (2018) studied on prediction of wheel and rail wear under different contact conditions using artificial neural networks. Serafińska *et al*. (2018) used artificial neural network in their study about friction law for elastomeric materials applied in finite element sliding contact simulations. Aleksendrića and Barton (2009) studied about prediction of disc brake performance by using artificial neural network. Rapettoa *et al*. (2009) studied about the influence of surface roughness on real area of contact in normal, dry, friction free, rough contact by using artificial neural network. Xiaoqiang *et al*. (2005) studied about solving elastoplastic contact problem by ANN.

As seen from the literature search, there is a clear gap about using artificial neural networks method for receding contact problem analysis. In this study, it is aimed to investigate if this method is proper and reliable to predict the dimensionless parameters related to the maximum contact pressures and contact areas of receding contact problem for two elastic layers whose elastic constants and heights are different supported by two elastic quarter planes. The more realistic and correct definition of the contact parameters such as normal contact stiffness, penetration limit, etc. and the contact algorithms in any commercial software are depending on the user experience with contact problems, where more and more experimentations carried out in well-equipped laboratories are the usual form to choose the contact parameters. An alternative used in this work to avoid experimentation is to employ artificial neural networks, where some results of the contact solution are used to estimate the contact parameters. The theoretical solution of the problem was obtained from the study by Yaylacı and Birinci (2013). The input and output values of the training and testing set patterns are modeled exercising the theoretical solution. The best result

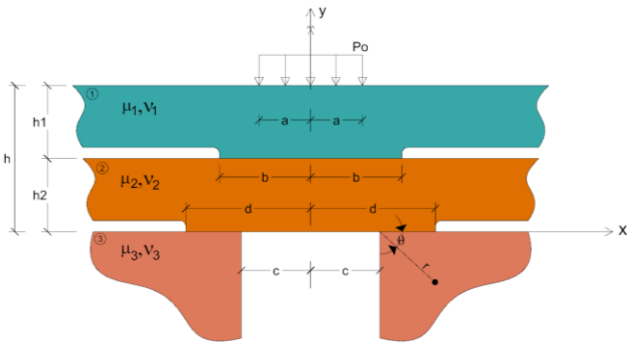

Fig. 1 Geometry and loading of the receding contact problem

and minimum ANN structure is determined by test and error. After training, the effects of some parameters on maximum contact stress and contact areas were compared with artificial neural network results and theoretical results.

2. Theoretical solution

Consider symmetric contact problem for the quarter planes and two elastic layers with different elastic constants and heights shown in Fig. 1. The upper elastic layer is subjected to symmetrical distributed load whose length is 2a on its top surface. It is assumed that contact between all surfaces is frictionless and the effect of gravity force is neglected. Upper layer and lower layer are in contact over the interval $(-b, b)$, the lower layer and quarter planes are in contact over the interval (c, d). The heights of the upper layer and lower layer are h_1 and h_2, respectively. μ_i and ν_i $(i = 1,2,3)$ are elastic constants of the layers and quarter planes. The subscript $i(i = 1,2,3)$ refers to the layers and quarter planes, respectively. Thickness in z-direction is taken to be unit.

The analytical solution of the problem considered by Yaylaci and Birinci (2013) is summarized in the following. The stress and the displacement expressions of the layers are obtained using theory of elasticity and integral transform technique as follows.

$$u_i(x,y) = \frac{2}{\pi}\int_0^\infty \left\{\left[A_i + B_i y\right]e^{-\alpha y} + \left[C_i + D_i y\right]e^{\alpha y}\right\}\sin(\alpha x)\,d\alpha \quad (1)$$

$$\mathrm{v}_i(x,y) = \frac{2}{\pi}\int_0^\infty \left\{\left[A_i + B_i\left(\frac{\kappa_i}{\alpha} + y\right)\right]e^{-\alpha y} + \left[-C_i + D_i\left(\frac{\kappa_i}{\alpha} - y\right)\right]e^{\alpha y}\right\}\cos(\alpha x)\,d\alpha \quad (2)$$

$$\frac{1}{2\mu_i}\sigma_{x_i}(x,y) = \frac{2}{\pi}\int_0^\infty \left\{\left[\alpha\left(A_i + B_i y\right) - \left(\frac{3-\kappa_i}{2}\right)B_i\right]e^{-\alpha y} + \left[\alpha\left(C_i + D_i y\right) + \left(\frac{3-\kappa_i}{2}\right)D_i\right]e^{\alpha y}\right\}\cos(\alpha x)\,d\alpha \quad (3)$$

$$\frac{1}{2\mu_i}\sigma_{y_i}(x,y) = \frac{2}{\pi}\int_0^\infty \left\{-\left[\alpha\left(A_i + B_i y\right) + \left(\frac{1+\kappa_i}{2}\right)B_i\right]e^{-\alpha y} + \left[-\alpha\left(C_i + D_i y\right) + \left(\frac{1+\kappa_i}{2}\right)D_i\right]e^{\alpha y}\right\}\cos(\alpha x)\,d\alpha \quad (4)$$

$$\frac{1}{2\mu_i}\tau_{xy_i}(x,y) = \frac{2}{\pi}\int_0^\infty \left\{-\left[\alpha\left(A_i + B_i y\right) + \left(\frac{\kappa_i - 1}{2}\right)B_i\right]e^{-\alpha y} + \left[\alpha\left(C_i + D_i y\right) - \left(\frac{\kappa_i - 1}{2}\right)D_i\right]e^{\alpha y}\right\}\sin(\alpha x)\,d\alpha \quad (5)$$

Where $u_i(x,y)$ and $\mathrm{v}_i(x,y)$ are the x and y components of the displacement vector and $\sigma_x(x,y), \sigma_y(x,y), \tau_{xy}(x,y)$ are the stress components of the layers. $\kappa_i = (3 - 4\nu_i)$ for plane strain and ν_i is the Poisson's ratio. A_i, B_i, C_i and D_i $(i = 1,2)$ are the unknown coefficients for the layers which will be determined from boundary conditions of the problem.

The stress and displacement expressions for the quarter planes can be written as follows

$$2\mu\left(\frac{\partial u_\theta}{\partial r}r^2\right)^M = s(s+1)i\left[F_1 e^{is\theta} - F_2 e^{-is\theta}\right] + \left[(s+1)(s+2) + (1-\nu)(-4s-4)\right]\left[G_1 e^{i(s+2)\theta} - G_2 e^{-i(s+2)\theta}\right] \quad (6)$$

$$\left(r^2\sigma_r\right)^M = \left(\frac{\partial^2}{\partial\theta^2} - s\right)\left[\phi^M\right] \quad (7)$$

$$\left(r^2\sigma_\theta\right)^M = s(s+1)\left[\phi^M\right] \quad (8)$$

$$\left(r^2\tau_{r\theta}\right)^M = (s+1)\frac{\partial}{\partial\theta}\left[\phi^M\right] \quad (9)$$

$$\phi^M(s,\theta) = F_1 e^{is\theta} + F_2 e^{-is\theta} + G_1 e^{i(s+2)\theta} + G_2 e^{-i(s+2)\theta} \quad (10)$$

Where, $\sigma_r(r,\theta), \sigma_\theta(r,\theta), \tau_{r\theta}(r,\theta)$ are the stress components for the quarter planes, u_θ is the transverse component of displacement normal to the radial direction and ϕ^M is Airy stress function.

Boundary conditions of the receding contact problem for the elastic layers can be written as

$$\tau_{xy}^{(1)}(x,h) = 0,\ (0 \le x < \infty) \quad (11)$$

$$\sigma_y^{(1)}(x,h) = \left\{\begin{matrix} -p_0,\ (0 \le x < a) \\ 0,\ (a \le x < \infty)\end{matrix}\right\} \quad (12)$$

$$\tau_{xy}^{(1)}(x,h_2) = 0, (0 \le x < \infty) \quad (13)$$

$$\tau_{xy}^{(2)}(x,h_2) = 0, (0 \le x < \infty) \quad (14)$$

$$\sigma_y^{(1)}(x,h_2) = \left\{\begin{matrix} -p_1(x), (0 \le x < b) \\ 0, (b \le x < \infty)\end{matrix}\right\} \quad (15)$$

$$\sigma_y^{(1)}(x,h_2) = \sigma_y^{(2)}(x,h_2), (0 \le x < \infty) \quad (16)$$

$$\sigma_y^{(2)}(x,0) = \left\{\begin{matrix} -p_2(x), (c < x < d) \\ 0, \left(0 \le x \le c\ ,\ \ d \le x < \infty\right)\end{matrix}\right\} \quad (17)$$

$$\tau_{xy}^{(2)}(x,0) = 0, (0 \le x < \infty) \quad (18)$$

$$\frac{\partial \mathrm{v}_2(x,0)}{\partial x} = \frac{\partial u_\theta}{\partial r}, (c < x < d) \quad (19)$$

$$\frac{\partial}{\partial x}\left[\mathrm{v}_1(x,h_2) - \mathrm{v}_2(x,h_2)\right] = 0, (0 \le x < b) \quad (20)$$

For the quarter planes, the boundary conditions in polar coordinates are

$$\sigma_\theta(r,\theta) = -p_2(r), (c < r < d), (\theta = 0) \quad (21)$$

$$\tau_{r\theta}(r,\theta) = 0, (d < r < \infty), (\theta = 0) \quad (22)$$

$$\sigma_\theta(r,\theta) = 0, (0 < r < \infty), (\theta = \pi/2) \quad (23)$$

$$\tau_{r\theta}(r,\theta)=0,(0<r<\infty),(\theta=\pi/2) \tag{24}$$

Equilibrium conditions of the problem may be expressed as

$$\int_{-b}^{b} p_1(x_1)dx_1 = 2ap_0 \tag{25}$$

$$\int_{c}^{d} p_2(x_2)dx_2 = ap_0 \tag{26}$$

Where p_0 is a known distributed load, $p_1(x)$ and $p_2(x)$ are the unknown contact pressures on the contact areas (b) and $(d-c)$, respectively.

By using boundary conditions (11-18), A_i, B_i, C_i and D_i $(i=1,2)$ coefficients can be determined in terms of $p_1(x)$ and $p_2(x)$. Substituting Eqs. (21-24) into stress and displacement expressions (6-10) and by using Mellin transform technique, expression $\partial u_\theta/\partial r$ in Eq. (19) is obtained. By substituting A_i, B_i, C_i and D_i $(i=1,2)$ coefficients and expression $\partial u_\theta/\partial r$ into Eqs. (19-20), after some routine manipulations and using the symmetry conditions $p_1(x)=p_1(-x)$, $p_2(x)=p_2(-x)$ one may obtain following the system of singular integral equations.

$$\begin{aligned}&\frac{1}{\pi}\int_{-b}^{b}\left[\frac{1}{t-x}-M_{11}(x,t)-R_{11}(x,t)\right]p_1(t_1)dt_1\\&+\frac{1}{\pi}\int_{c}^{d}R_{12}(x,t)p_2(t_2)dt_2=\frac{1}{\pi}p_0M(x)\end{aligned} \tag{27}$$

$$\begin{aligned}&\frac{1}{\pi}\int_{-b}^{b}M_{21}(x,t)p_1(t_1)dt_1+\frac{1}{\pi}\int_{c}^{d}\left[\frac{1}{t+x}-\frac{1}{t-x}+\right.\\&\left.M_{22}(x,t)-\frac{\mu_2}{\mu_3}\frac{1+\kappa_3}{1+\kappa_2}k_{22}(x,t)\right]p_2(t_2)dt_2=0\end{aligned} \tag{28}$$

Where $M_{11}(x_1,t_1)$, $R_{11}(x_1,t_1)$, $R_{12}(x_1,t_2)$, $M_{21}(x_2,t_1)$, $M_{22}(x_2,t_2)$, $k_{22}(x_2,t_2)$, $M(\alpha)$ are explained by Yaylaci and Birinci (2013).

The numerical solutions of the integral equations will be achieved by Gauss-Jacobi Integration Formulation which is given in Krenk (1975) and Erdogan *et al*. (1973).

To simplify the numerical analysis of the integral equation, the following dimensionless quantities can be introduced.

$$\alpha=\frac{z}{h_2} \tag{29}$$

$$t_1=br_1,\ t_2=\frac{d-c}{2}r_2+\frac{d+c}{2} \tag{30}$$

$$x_1=bs_1,\ x_2=\frac{d-c}{2}s_2+\frac{d+c}{2} \tag{31}$$

$$g(r_1)=\frac{p_1(br_1)}{p_0},\ g(r_2)=\frac{p_2\left(\frac{d-c}{2}r_2+\frac{d+c}{2}\right)}{p_0} \tag{32}$$

Substituting these dimensionless quantities given in (29-31) into (25-28) these equations may be written as follows

$$\frac{1}{\pi}\int_{-1}^{1}\left[\frac{1}{r_1-s_1}-\bar{M}_{11}(s,r)-\bar{R}_{11}(s,r)\right]g_1(r_1)dr_1+\frac{1}{\pi}\int_{-1}^{1}\bar{R}_{12}(s,r)g_2(r_2)dr_2=\frac{1}{\pi}\bar{M}(s_1) \tag{33}$$

$$\begin{aligned}&\frac{1}{\pi}\int_{-1}^{1}\bar{M}_{21}(s,r)g(r_1)dr_1+\\&\frac{1}{\pi}\int_{-1}^{1}\left[\frac{1}{(r_2+s_2)+2(\frac{d+c}{d-c})}-\frac{1}{(r_2-s_2)}+\right.\\&\left.\bar{M}_{22}(s,r)-\frac{\mu_2}{\mu_3}\frac{1+\kappa_3}{1+\kappa_2}k_{22}(s,r)\right]g(r_2)dr_2=0\end{aligned} \tag{34}$$

$$\frac{b}{2a}\int_{-1}^{1}g_1(r_1)dr_1=1 \tag{35}$$

$$\frac{d-c}{2a}\int_{-1}^{1}g_2(r_2)dr_2=1 \tag{36}$$

Where,
$\bar{M}_{11}(s,r),\bar{R}_{11}(s,r),\bar{R}_{12}(s,r),\bar{M}_{21}(s,r),\bar{M}_{22}(s,r),\bar{k}_{22}(s,r),\bar{M}(s)$ are explained by Yaylaci and Birinci (2013).

One may be noticed that because of the smooth contact at the end point b, the unknown function $p_1(x)$ is zero at the ends, thereby the index of integral equation (33) is "-1". Its solution may be expressed as

$$g_1(r_1)=G_1(r_1)(1-r_1^2)^{-1/2},(-1\le r_1\le 1) \tag{37}$$

Using the Gauss-Jacobi integration formulas, the integral Eq. (33) and equilibrium conditions (35) become

$$\sum_{i=1}^{N}W_{1i}^{N}\left[\frac{1}{r_{1i}-s_{1k}}+k_{11}(s_{1k},r_{1i})\right]G_1(r_{1i})+\sum_{i=1}^{N}W_{2i}^{N}\bar{R}_{12}(s_{1k},r_{2i})G_2(r_{2i})=\frac{1}{\pi}\bar{M} \tag{38}$$
$(k=1,2,...,N+1)$

$$\frac{b}{2a}\sum_{i=1}^{N}W_{1i}^{N}G_1(r_{1i})-\frac{1}{\pi}=0 \tag{39}$$

r_{1i} and s_{1k} are the roots of the related Jacobi polynomials and W_{1i}^{N} is the weighting constant

$$r_{1i}=\cos\left(\frac{i\pi}{N+1}\right),(i=1,2,...,N) \tag{40}$$

$$s_{1k}=\cos\left(\frac{\pi}{2}\frac{2k-1}{N+1}\right),(k=1,2,...,N+1) \tag{41}$$

$$W_{1i}^{N}=\frac{1-r_{1i}^2}{N+1},\ (i=1,2,...,N) \tag{42}$$

One may be noticed that because of the smooth contact at the end point d, unknown functions $p_2(x)$ is zero at the ends. Unknown function $p_2(x)$ is infinite in the point c which in the interior edge of the quarter plane, thereby the index of integral Eq. (34) is "0". Its solution may be expressed as

$$g_2(r_2)=G_2(r_2)(1-r_2)^{-1/2}(1+r_2)^{\beta_2},(-1\le r_2\le 1) \tag{43}$$

Where β_2 can be obtained as follows.

$$\begin{aligned}&\frac{\mu_2}{\mu_3}\frac{1+\kappa_3}{1+\kappa_2}\left(2\lambda^2-1+\cos\pi\lambda\right)\cos\pi\lambda-\sin^2\pi\lambda=0\\&\beta_2=\lambda_1-1\end{aligned} \tag{44}$$

Using the Gauss-Jacobi integration formulas the integral Eq. (34) and equilibrium conditions (36) become

$$\sum_{i=1}^{N}W_{1i}^{N}\bar{\bar{M}}_{21}(s_{2k},r_{1i})G_1(r_{1i})+\sum_{i=1}^{N}W_{2i}^{N}\left[-\frac{1}{r_{2i}-s_{2k}}+K_{22}(s_{2k},r_{2i})\right]G_2(r_{2i})=0 \tag{45}$$
$(k=1,2,...,N+1)$

$$\frac{d-c}{2a}\sum_{i=1}^{N} W_{2i}^{N} G_2(r_{2i}) - \frac{1}{\pi} = 0 \tag{46}$$

Where r_{2i} and s_{2k} are the roots of the related Jacobi polynomials and W_{2i}^{N} is the weighting constant

$$P_N^{(\alpha_2,\beta_2)}(r_{2i}) = 0, (i = 1,2,...,N) \tag{47}$$

$$P_N^{(\alpha_2-1,\beta_2-1)}(s_{2k}) = 0, (k = 1,2,...,N) \tag{48}$$

$$W_{2i}^{N} = -\frac{1}{\pi}\frac{2N+\alpha_2+\beta_2+2}{(N+1)!(N+\alpha_2+\beta_2+1)} \frac{\Gamma(N+\alpha_2+1)\Gamma(N+\beta_2+1)}{\Gamma(N+\alpha_2+\beta_2+1)} \frac{2^{\alpha_2+\beta_2}}{P_N^{(\alpha_2+\beta_2)}(r_{2i})P_{N+1}^{(\alpha_2+\beta_2)}(r_{2i})} \tag{49}$$

It can be seen that the extra Eqs. in (38) and (45) correspond to the consistency condition of the original integral Eqs. (33) and (34). It may be also shown that the $(N/2+1)$-th equations in (38) and (45) are automatically satisfied. Thus, Eqs. (38), (39), (45) and (46) give $2N+2$ algebraic equations to determine the $2N+2$ unknowns $G_1(r_{1i})$ and $G_2(r_{2i})$, b and $(d-c)$. The system of equations are linear $G_1(r_{1i})$ and $G_2(r_{2i})$, but highly nonlinear in b and $(d-c)$. Therefore, an interpolation and iteration scheme had to be used to obtain these two unknowns.

3. Application of the artificial neural network

Artificial neural network is a logical programming technique developed by imitating the working mechanism of brain. It makes decisions, draws conclusions, achieves results from the existing information in case of insufficient data, and accepts continuous data input, learns and remembers.

The architecture is composed of a number of basic units called neuron or processing unit. Neurons are functionally simple, but highly interconnected, which are normally organized into layers (Dawson and Wilby 2009). Every neuron may have several input paths. The weighted values of the input paths are combines by a simple summation. The combined input-weight values are then modified by activation function during training to better reproduce output (Çakıroğlu *et al*. 2005). Fig. 2 shows the basics of an artificial neuron.

A general artificial neural network system consists of layers. The input layer receives information from the external environment. There is no transaction in this layer. The hidden layer processes the information from the input layer. It can contain more than one layer. The output layer takes the weighted sum of the outputs of all hidden layer neurons and produces the output of the model. Each neuron is independent in its layer but is connected to all neurons in a next layer with weights (Çakıroğlu *et al*. 2005). The number of neurons in the input and output layers is decided according to the requirements in the problem but there is no rule in determining the number of process elements in the hidden layers. The best generalization performance is obtained by trial and error against network complexity (Le Cun *et al*. 1990).

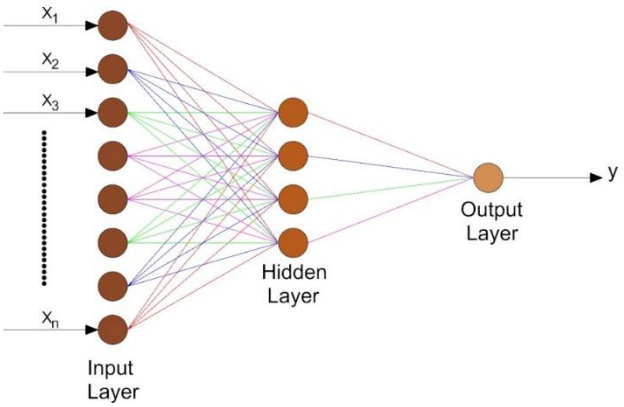

Fig. 2 Artificial neuron

Neural network learning process takes place in two ways; such as supervised and unsupervised. MLP is the most popular supervised learning approach due to its clear architecture and comparably simple algorithm (Yan *et al*. 2006). After the MLP architecture has been determined, the connection weights of the network must be computed with a training procedure based on training models and desired output.

MLP should normalize the values in the dataset for best results. If the training set [0.1-0.9] was normalized within the range that will remain within the sigmoid activation function. It was observed that the training results with the desired sensitivity were reached quickly (Zurada 1992).

ANN architecture

The input data used for the training of the network has been obtained from theoretical solutions. Network models were constructed using 6 process pattern. These input variables are,

a/h_2: Length of distributed load

c/h_2: Distance between the two quarter planes

h_1/h_2: Ratio of lower and upper elastic layer heights

μ_2/μ_1: Ratio of upper and lower elastic layer shear modulus

μ_3/μ_2: Ratio of quarter planes and lower elastic layer shear modulus

$\kappa_1=\kappa_2=\kappa_3$: Elastic constants of the layers and quarter planes

The output layer consists of 4 different processing elements. These are:

$P_1^{\max}(x)/P_0$: Dimensionless parameter related to the maximum contact pressure between two layers

$P_2^{\max}(x)/P_0$: Dimensionless parameter related to the maximum contact pressure between the lower layer and quarter plane

b/h_2: Dimensionless parameter related to the contact areas between two layers

$(d-c)/h_2$: Dimensionless parameter related to the contact areas between the lower layer and quarter plane.

The MLP used in this study is consisted of three-layer including an input layer, a hidden layer, and an output layer. In this study Statistica 12 applications were used for data processing and the design of artificial neural networks. 173

Table 1 Test parameters

c/h_2	$\kappa_2 = \kappa_3$	$\frac{a}{h_2}$	$\frac{h_1}{h_2}$	$\frac{\mu_2}{\mu_1}$	$\frac{\mu_3}{\mu_2}$
0.01	1.25	0.1	0.1	0.25	0.25
0.02	2.0	0.2	0.2	0.5	0.5
0.03	2.5	0.3	0.3	0.75	0.75
0.04		0.4	0.4	1	1
0.05		0.5	0.5	2	2
0.075		0.6	0.6	3	4
0.1		0.7	0.7	4	5
0.2		0.8	0.8	5	8
0.3		0.9	0.9	6	10
0.4		1	1	7	
0.5			1.1	8	
0.6			1.2	9	
0.7			1.3	10	
0.75			1.4		
0.8			1.5		
0.9			1.6		
1			1.7		
			1.8		
			1.9		
			2		

patterns which are different combinations of the values in Table 1 are solved theoretically to form the training set. Only 18 input values and the desired outputs of the validation set are given in Appendix 1. Variables were normalized to the interval [0, 1]. The input and output values of each patterns were normalized at different ranges. The input variables were divided randomly into 3 groups by the program: 70% for learning group, 15% for testing group and %15 for validation group.

The number of neurons in a hidden layer will significantly influence the network's ability to generalize from the training data to the unknown patterns (Kavzoglu, 2001). Some problems require more than one hidden layer to train a network properly, whereas others require only one hidden layer. Accuracy and convergence speed are the two main parameters of a network. In our study network is tested for different number of hidden layer units. 2-10 units are used in the hidden layer to find optimum number.

The weights are initialized into randdom values between 0.0001 and 0.001. Then compared the appropriateness of both available error functions, the sum of squares and entropy, during training. After selecting the network type, network activation functions which transfer the incoming signals of the previous layer to the next layer using a mathematical function are selected. In our work, we

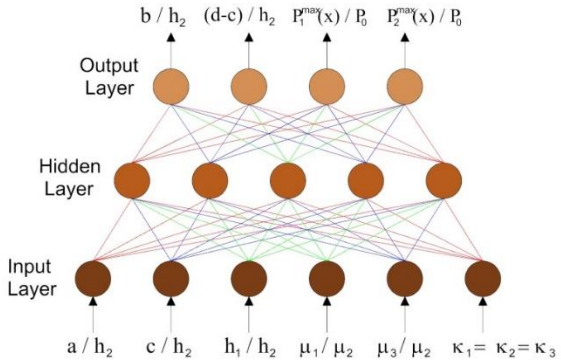

Fig. 3 System architecture

selected all function types (Identity, Logistic sigmoid, Hyperbolic tangent, Exponential, Softmax, and Gaussian) for input and output. The output layer consisted of nodes. The architecture of the overall decision support system is illustrated in Fig. 3. Then network architectured with the BFGS (Broyden fletcher goldfarb shanno) algoritm. Finally, neural network architecture was formed with the variables selected in the previous step, and 5000 networks were trained and retained for further evaluation. There are many computer programs used this method. In this study, a computer program written in C++ language was used to calculate the contact areas and contact pressures. A flow chart of the ANN design is shown in Appendix 2.

4. Numerical results

In this study, whether neural network analysis can be used to estimate contact pressures and contact areas by using a/h_2, c/h_2, h_1/h_2, μ_2/μ_1, μ_3/μ_2 and $\kappa_1=\kappa_2=\kappa_3$. Results show that neural network analysis appears to be robustly capable of predicting the contact pressures and contact areas correctly. This option offers a simple and affordable approach for quick estimation.

The MLP network type, with the error term *sos* produced superior networks. The most appropriate network configuration was 10 units for each hidden layer with *tanh* activation function. The quality of the network was evaluated based on the error rate of the validation group, as described in Adamus-Bialek *et al* (2017). The best of the neural networks recognized are shown in Table 2.

The relative error is determined as

$$e_{rel} = \left| \frac{O_{Actual} - O_{ANN}}{O_{Actual}} \right| x100 \tag{50}$$

Table 2 The characteristics of artificial networks that recognize b/h_2, $(d-c)/h_2$, $P_1^{\max}(x)/P_0$, $P_2^{\max}(x)/P_0$

Network	MLP	Error in learning (%)	Error in learning testing (%)	Error in learning validation(%)	Learning algorithm	Error function	Activation function in hidden layer	Activation function in output layer
N 1	6-10-1	1.16	0.04	5.15	BFGS 514	SOS	Tanh	Exponential
N 2	6-10-1	1.91	0	0	BFGS 280	SOS	Tanh	Identity
N 3	8-10-1	4.34	2.15	0	BFGS 601	SOS	Tanh	Identity
N 4	8-10-1	0	0.02	0	BFGS 368	SOS	Logistic	Exponential

BFGS: Broyden fletcher goldfarb shanno algorithm, SOS: Sum of square, Tanh: hyperbolic tangent function

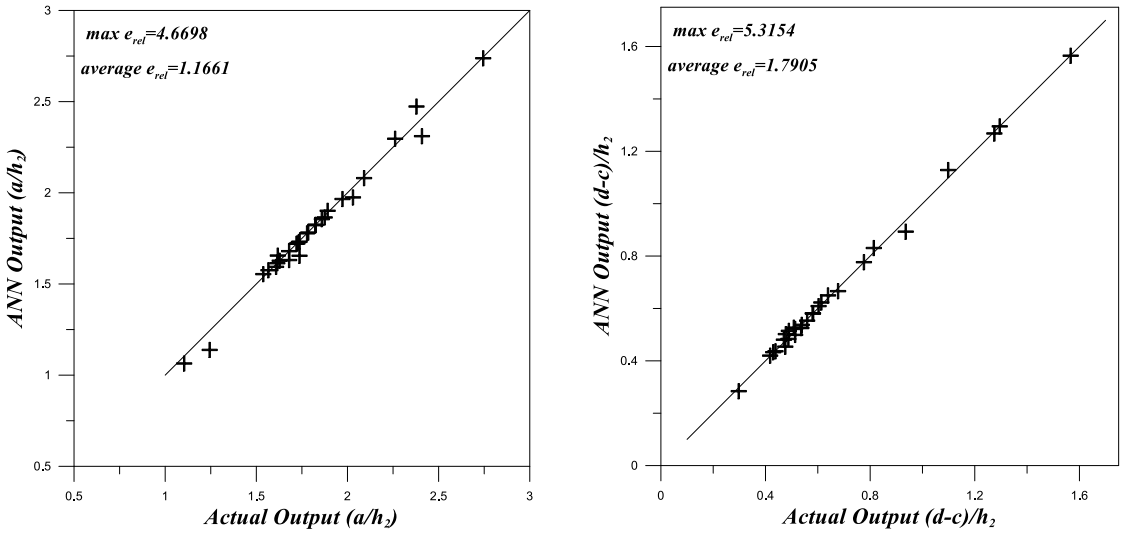

(a) (b)

Fig. 4 Comparison of contact areas obtained from ANN and theoretical solution

Table 3 Variations of the contact areas with distance between the two quarter planes (a/h_2=1, h_1/h_2=1, μ_2/μ_1=2, μ_3/μ_2=2, κ_1=κ_2=κ_3=2)

$\frac{c}{h_2}$	b/h_2			$(d-c)/h_2$		
	Actual Output	ANN Output	e_{rel}	Actual Output	ANN Output	e_{rel}
0.2	1.6153	1.614847	0.0280	1.5666	1.565726	0.0558
0.4	1.6279	1.628649	0.0460	1.2953	1.295919	0.0478
0.8	1.7205	1.721453	0.0554	0.7762	0.777329	0.1455
1.0	1.8247	1.824764	0.0035	0.5812	0.581814	0.1056
1.2	1.9726	1.966988	0.2845	0.4381	0.437074	0.2342
1.5	2.2614	2.297653	1.6031	0.2976	0.284811	4.4974

Where O_{actual} and O_{ANN} are the theoretical solution and ANN prediction of the b/h_2, $(d-c)/h_2$, $P_1^{max}(x)/P_0$, $P_2^{max}(x)/P_0$.

The maximum relative errors of the a/h_2 and $(d-c)/h_2$ are calculated as 4.6698% and 5.3154% (Fig. 4).

The testing set is used to evaluate the capacity of the trained ANN structure. Variations of the contact areas (b/h_2) and $((d-c)/h_2)$ with distance between the two quarter planes (c/h_2), with elastic constants (μ_2/μ_1), with length of distributed load (a/h_2), with (h_1/h_2), and with $\kappa_2 = \kappa_3$ are given in Table 3 to Table 7, respectively. The maximum relative errors of the $P_1^{\max}(x)/P_0$ and $P_2^{\max}(x)/P_0$ in the testing set are calculated as 4.874% and 4.690%, respectively and Fig. 4 is an expression of the learning capacity of the network on the $P_1^{\max}(x)/P_0$ and $P_2^{\max}(x)/P_0$. Each point stands for a testing pattern output. The nearer the points gather around the diagonal, the better are the learning results.

In the following, the trained architecture is used to predict the effect of some factors on the dimensionless parameters related to the contact areas b/h_2 and $(d-c)/h_2$ and the results are compared with theoretical solutions.

In Table 3, the contact areas between two elastic layers (b/h_2) and between the lower layer and quarter planes $((d-c)/h_2)$ are analyzed by depending on the various of distance value between the two quarter planes (c/h_2).

Table 4 Variations of contact areas with elastic constant (a/h_2=1, c/h_2=1, h_1/h_2=1, μ_3/μ_2=2, κ_1=κ_2=κ_3=2)

$\frac{\mu_2}{\mu_1}$	b/h_2			$(d-c)/h_2$		
	Actual Output	ANN Output	e_{rel}	Actual Output	ANN Output	e_{rel}
2	1.8247	1.824764	0.0035	0.5812	0.581814	0.1056
3	1.7370	1.655886	4.6698	0.5364	0.525960	1.9463
4	1.6799	1.632288	2.8342	0.5132	0.522420	1.7966
6	1.6085	1.595044	0.8366	0.4892	0.515203	5.3154
8	1.5663	1.576457	0.6485	0.4776	0.502680	5.2513
10	1.5382	1.555033	1.0943	0.4701	0.481466	2.4178

Table 5 Variations of contact areas with length of distributed load (c/h_2=1, h_1/h_2=1, μ_2/μ_1=2, μ_3/μ_2=2, κ_1=κ_2=κ_3=2)

$\frac{a}{h_2}$	b/h_2			$(d-c)/h_2$		
	Actual Output	ANN Output	e_{rel}	Actual Output	ANN Output	e_{rel}
0.2	1.7256	1.723608	0.1154	0.4756	0.454789	4.3757
0.4	1.7331	1.731224	0.1082	0.4874	0.484304	0.6352
0.8	1.7784	1.778814	0.0233	0.5385	0.538148	0.0654
1.2	1.8912	1.902573	0.6014	0.6388	0.650509	1.8330
1.6	2.0912	2.081604	0.4589	0.8139	0.831405	2.1508
2.0	2.3786	2.474297	4.0232	1.0983	1.129139	2.8079

With increasing distance between the two quarter planes, the contact area between the elastic layers increases. On the contrary, the contact area between the lower layer and two quarter planes decreases.

Table 4 shows variations of the contact areas b/h_2 and $(d-c)/h_2$ with ratios of the elastic constants (μ_2/μ_1). In Table 2, the contact areas between layers b/h_2 and between lower layer quarter planes $(d-c)/h_2$ decrease with increasing (μ_2/μ_1).

Table 5 shows the variation of size of the contact areas b/h_2 and $(d-c)/h_2$ for various values of length of distributed load (a/h_2). With increasing length of distributed load, the contact area between the elastic layers and contact area between the lower layer and the two quarter planes increase.

Table 6 Variations of contact areas with h_1/h_2 (a/h_2=1, c/h_2=1, μ_2/μ_1=2, μ_3/μ_2=2, $\kappa_1=\kappa_2=\kappa_3$=2)

$\frac{h_1}{h_2}$	b/h_2			$(d-c)/h_2$		
	Actual Output	ANN Output	e_{rel}	Actual Output	ANN Output	e_{rel}
0.2	1.1043	1.065039	3.5553	0.4177	0.420590	0.6919
0.4	1.2441	1.199500	3.5849	0.4295	0.433581	0.9502
0.8	1.6176	1.656844	2.4261	0.5082	0.527338	3.7658
1.2	2.0302	1.975803	2.6794	0.6774	0.666778	1.5681
1.6	2.4086	2.311551	4.0293	0.9360	0.893948	4.4927
2.0	2.7446	2.738855	0.2093	1.2749	1.268815	0.4773

Table 7 Variations of contact areas with $\kappa_2=\kappa_3$ (a/h_2=1, c/h_2=1, μ_2/μ_1=2, μ_3/μ_2=2, κ_1=2, h_1/h_2=1)

$\kappa_2=\kappa_3$	b/h_2			$(d-c)/h_2$		
	Actual Output	ANN Output	e_{rel}	Actual Output	ANN Output	e_{rel}
0.5	1.6799	1.680959	0.0630	0.5132	0.499742	2.6224
1.0	1.7372	1.732545	0.2680	0.5364	0.526762	1.7968
1.5	1.7846	1.782935	0.0933	0.5591	0.554161	0.8834
2.0	1.8247	1.824764	0.0035	0.5812	0.581814	0.1056
2.5	1.8593	1.856492	0.1510	0.6028	0.609599	1.1279
2.75	1.8750	1.865939	0.4833	0.6134	0.623503	1.6470

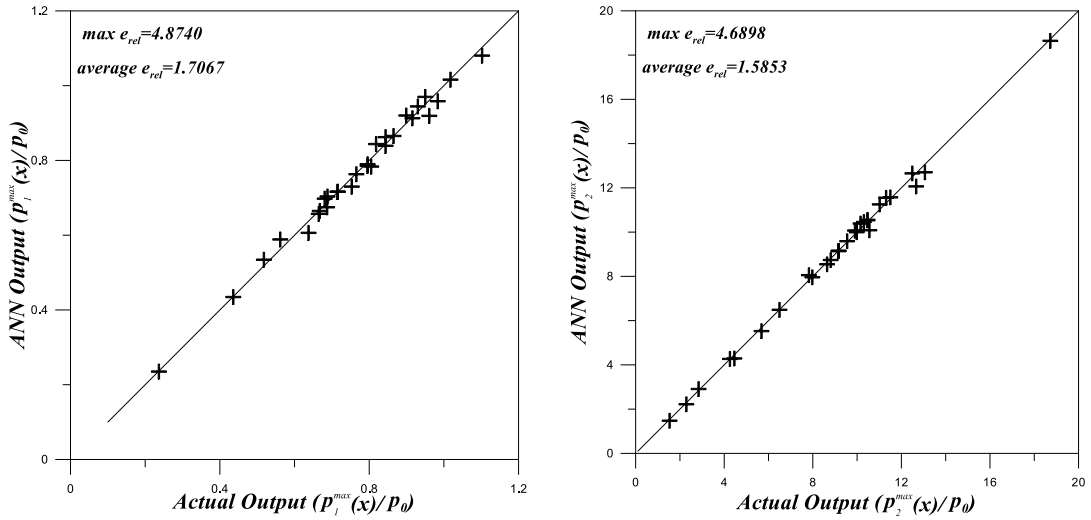

(a) (b)

Fig. 5 Comparison of obtained $P_1^{\max}(x)/P_0$ and $P_2^{\max}(x)/P_0$ from ANN prediction and theoretical solution

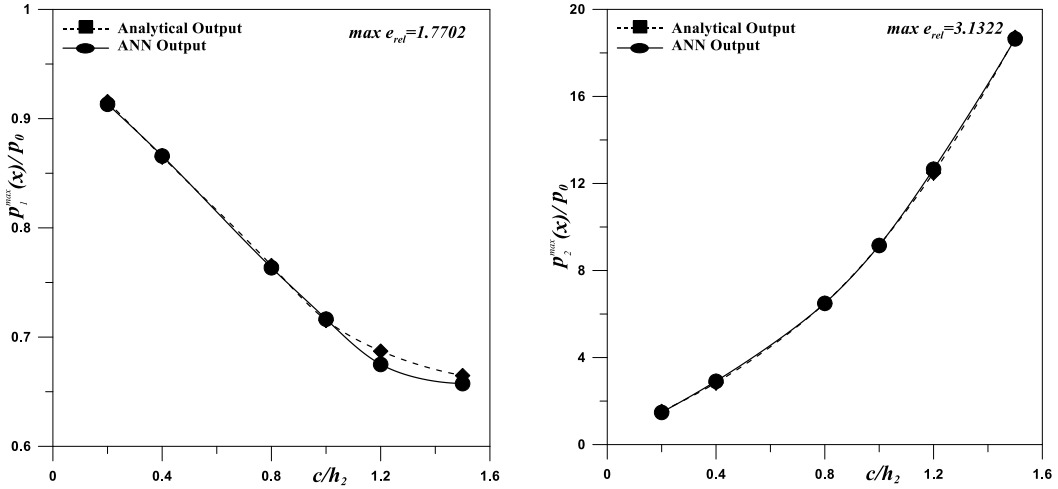

Fig. 6 Variations of the contact pressures $P_1^{\max}(x)/P_0$ and $P_2^{\max}(x)/P_0$ with distance between the two quarter planes (c/h_2), $(a/h_2 = 1, h_1/h_2 = 1, \mu_2/\mu_1 = 2, \mu_3/\mu_2 = 2, \kappa_1 = \kappa_2 = \kappa_3 = 2)$

Variations of the contact areas b/h_2 and $(d\text{-}c)/h_2$ with h_1/h_2 are given in Table 6. In the table, as h_1/h_2 increases, the contact areas b/h_2 and $(d\text{-}c)/h_2$ increase.

In Table 7, the contact areas between two elastic layers b/h_2 and between the lower layer and quarter planes $(d\text{-}c)/h_2$ are analyzed for quantities of the materials (κ_2, κ_3). With increasing quantities of the materials, the contact areas b/h_2 and $(d\text{-}c)/h_2$ increase.

Although contact pressure between the layers reaches its maximum value at the axis of symmetry, its value is zero at the endpoints of contact $(x = \pm b)$. Furthermore, contact pressures are zero at the points $(x = \pm d)$ where the quarter planes are separated from the lower layer and, theoretically, go to infinity at the inner edge $(x = \pm c)$ of the quarter planes.

Fig. 6 demonstrates the variation of $P_1^{\max}(x)/P_0$ and

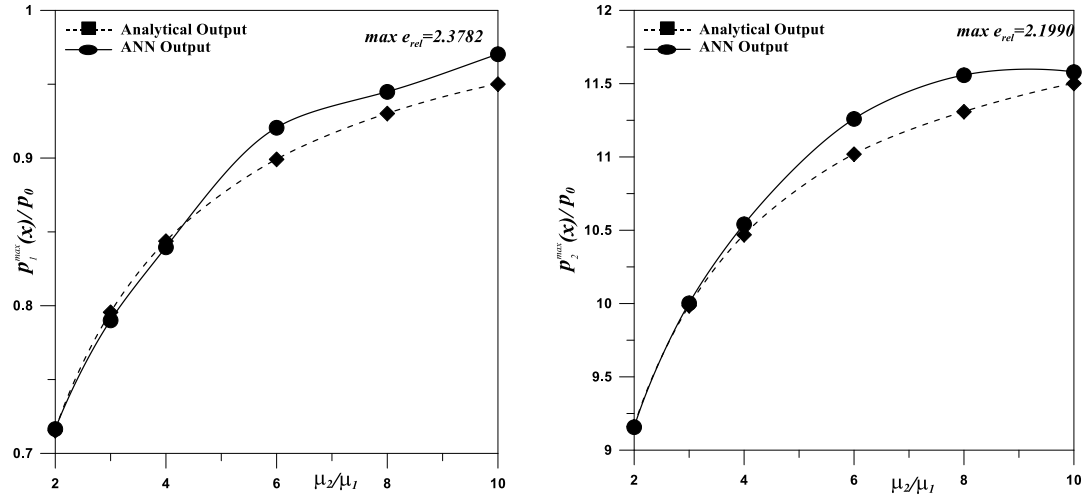

Fig. 7 Variation of the contact pressures $P_1^{\max}(x)/P_0$ and $P_2^{\max}(x)/P_0$ with elastic constants (μ_2/μ_1),$(a/h_2 = 1, c/h_2 = 1, h_1/h_2 = 1, \mu_3/\mu_2 = 2, \kappa_1 = \kappa_2 = \kappa_3 = 2)$

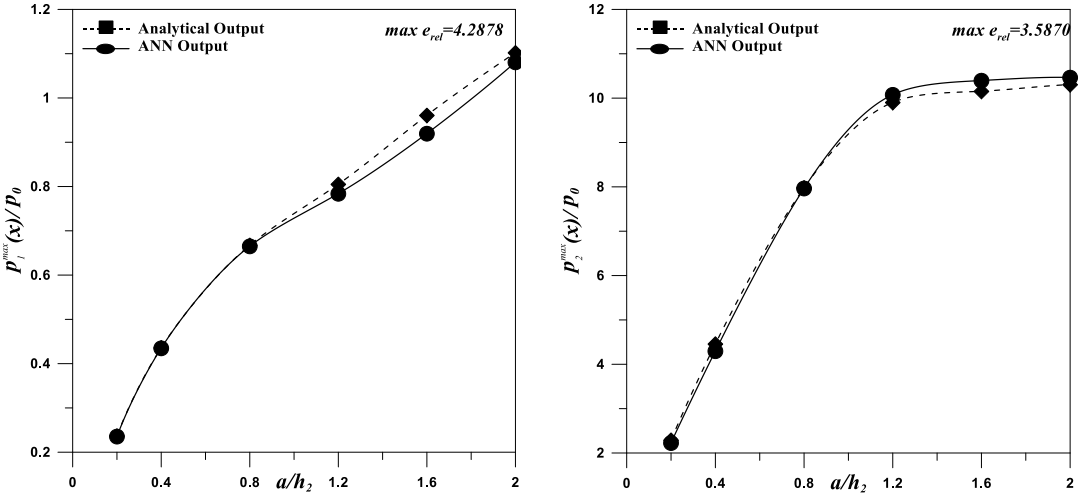

Fig. 8 Variation of the contact pressures $P_1^{\max}(x)/P_0$ and $P_2^{\max}(x)/P_0$ with length of distributed load (a/h_2), $(c/h_2 = 1, h_1/h_2 = 1, \mu_2/\mu_1 = 2, \mu_3/\mu_2 = 2, \kappa_1 = \kappa_2 = \kappa_3 = 2)$

$P_2^{\max}(x)/P_0$ with c/h_2 = (0.20, 0.40, 0.80, 1.00, 1.20, 1.50) for $(a/h_2 = 1, h_1/h_2 = 1, \mu_2/\mu_1 = 2, \mu_3/\mu_2 = 2, \kappa_1 = \kappa_2 = \kappa_3 = 2)$. It is seen that as c/h_2 increases, while the other input values are fixed, $P_1(x)/P_0$ decrease and $P_2(x)/P_0$ increase. Pattern input values are also selected different from those in the train and test sets. Maximum relative errors are 1.770% and 3.132%, respectively. The contact pressure distributions for various values of c/h_2 are shown in Fig. 6. With increasing distance between the two quarter planes, the contact pressure $P_1^{\max}(x)/P_0$ decreases. On the contrary, the contact pressure $P_2^{\max}(x)/P_0$ increases.

Fig. 7 demonstrates the variation of $P_1^{\max}(x)/P_0$ and $P_2^{\max}(x)/P_0$ with elastic constants $\mu_2/\mu_1 = 2.00, 3.00, 4.00, 6.00, 8.00, 10.00$ for a/h_2=1, c/h_2=1, h_1/h_2=1, $\mu_3/\mu_2 = 2$, $\kappa_1 = \kappa_2 = \kappa_3 = 2$. It is seen that as μ_2/μ_1 increases, while the other input values are fixed, $P_1^{\max}(x)/P_0$ and $P_2^{\max}(x)/P_0$ increase. Pattern input values are also selected different from those in the train and test sets. Maximum relative errors are 2.378% and 2.199%, respectively. Fig. 7 shows $P_1^{\max}(x)/P_0$ and $P_2^{\max}(x)/P_0$ the dimensionless maximum contact pressure distributions. In the event of increase lower layer and upper layer ratio shear modules, it is indicated that the contact pressure distributions at the contact surfaces between two elastic layers and between the lower layer and quarter plane increase.

Fig. 8 shows the variation of $P_1^{\max}(x)/P_0$ and $P_2^{\max}(x)/P_0$ with length of distributed load a/h_2=0.20, 0.40, 0.80, 1.20, 1.60, 2.00 for $c/h_2 = 1, h_1/h_2 = 1, \mu_2/\mu_1 = 2, \mu_3/\mu_2 = 2, \kappa_1 = \kappa_2 = \kappa_3 = 2$. It is seen that as a/h_2 increases, while the other input values are fixed, $P_1^{\max}(x)/P_0$ and $P_2^{\max}(x)/P_0$ increase. Pattern input values are also selected different from those in the train and test sets. Maximum relative errors are 4.288% and 3.587%, respectively. Fig. 8 shows the maximum contact pressure distributions $P_1^{\max}(x)/P_0$ and $P_2^{\max}(x)/P_0$ with variations of load width a/h_2. In the event of increased load width, it is indicated that the contact pressure distributions at the contact surfaces between the two elastic layers and between the lower layer and quarter plane increase.

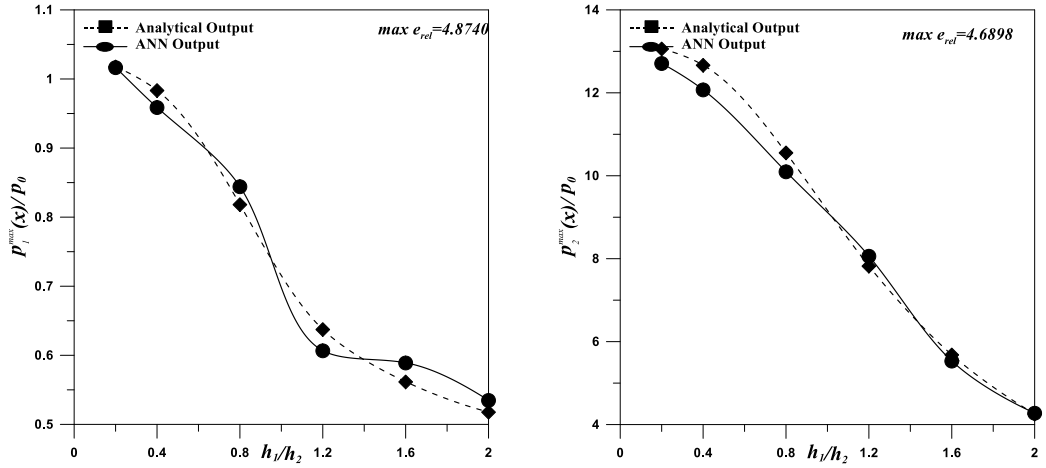

Fig. 9 Variation of the contact pressures $P_1^{\max}(x)/P_0$ and $P_2^{\max}(x)/P_0$ with (h_1/h_2), $(a/h_2 = 1, c/h_2 = 1, \mu_2/\mu_1 = 2, \mu_3/\mu_2 = 2, \kappa_1 = \kappa_2 = \kappa_3 = 2)$

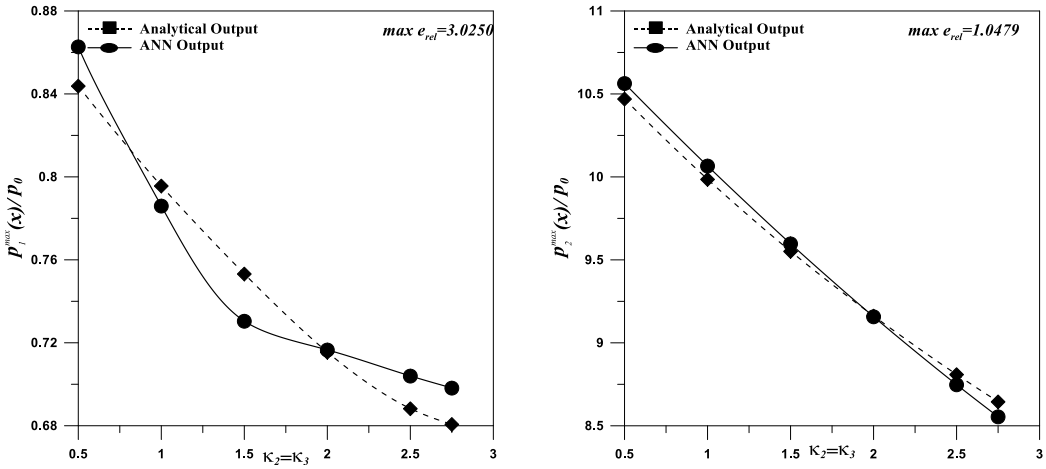

Fig. 10 Variation of the contact pressures $P_1^{\max}(x)/P_0$ and $P_2^{\max}(x)/P_0$ with $\kappa_2 = \kappa_3$, $(a/h_2 = 1, c/h_2 = 1, \mu_2/\mu_1 = 2, \mu_3/\mu_2 = 2, \kappa_1 = 2, h_1/h_2 = 1)$

Variation of $P_1^{\max}(x)/P_0$ and $P_2^{\max}(x)/P_0$ with h_1/h_2 = (0.20, 0.40, 0.80, 1.20, 1.60, 2.00) for $a/h_2 = 1, c/h_2 = 1, \mu_2/\mu_1 = 2, \mu_3/\mu_2 = 2, \kappa_1 = \kappa_2 = \kappa_3 = 2$ is given in Fig. 9. It is seen that as h_1/h_2 increases, while the other input values are fixed, $P_1^{\max}(x)/P_0$ and $P_2^{\max}(x)/P_0$ decrease. Pattern input values are also selected different from those in the train and test sets. Maximum relative errors are 4.874% and 4.690%, respectively. As seen in Fig. 9, the contact pressure $P_1^{\max}(x)/P_0$ decreases and $P_2^{\max}(x)/P_0$ increases with increasing of h_1/h_2.

Variation of $P_1^{\max}(x)/P_0$ and $P_2^{\max}(x)/P_0$ with $\kappa_2 = \kappa_3$ = (0.50, 1.00, 1.50, 2.00, 2.50, 2.75) for $a/h_2 = 1, c/h_2 = 1, \mu_2/\mu_1 = 2, \mu_3/\mu_2 = 2, \kappa_1 = 2, h_1/h_2 = 1$ is given in Fig. 10. It is seen that as κ_2, κ_3 increases, while the other input values are fixed, $P_1^{\max}(x)/P_0$ and $P_2^{\max}(x)/P_0$ decrease. Pattern input values are also selected different from those in the train and test sets. Maximum relative errors are 3.025% and 1.048%, respectively. The maximum contact pressure distributions for various values of $\kappa_2 = \kappa_3$ are shown in Fig. 10. In Fig. 10, $P_1^{\max}(x)/P_0$ and $P_2^{\max}(x)/P_0$ decrease with increasing $\kappa_2 = \kappa_3$.

5. Conclusions

The main purpose of this paper is to present a comparative study of the analytical method and the artificial neural network method for analyzing the receding contact problems. In this sense, a the MLP consisted of three-layer has been developed and verified to be very sufficient in predicting the dimensionless parameters related to the maximum contact pressures and contact areas of receding contact problem for two elastic layers whose elastic constants and heights are different supported by two elastic quarter planes. The training and test data sets for the contact areas, contact areas and the contact pressure distributions are derived analytically from the basic equations of elasticity. It is clearly observed that, number of processing elements in the hidden layer, initial weight values, learning rate and momentum term have considerable effects on the training. Dimensionless contact pressure distributions between two elastic layers $p_1(x)/p_0$ and between the quarter planes and the lower layer $p_2(x)/p_0$, contact areas (b/h_2) and $((d-c)/h_2)$ and the normal stress distributions $\sigma_x(0,y)/p_0$ and $\sigma_y(0,y)/p_0$ are derived for various dimensionless quantities, such as a/h_2, c/h_2,

h_1/h_2 and μ_2/μ_1. Obtained results show that load width, distance between the two quarter planes, material properties of layers and quarter planes and layers height ratio have considerable effect on the contact areas, the normal stress distribution and the contact pressure distribution. In addition, the part of obtaining results was shown that the artificial neural networks reduce the overall computation time required when compared with existing theoretical analysis methods. As a result of comparing study, it is shown that the artificial neural network predictions agree well with that of theoretical solutions in Figs. 4-10. Consequently, based on the figures above, application of artificial neural networks to contact problems can be practical especially for the time-consuming problems which require interpolation and iteration in theoretical solution. In this manner, the trained network can be used for on-line prediction of desired values of receding contact problems. ANNs may be applied to discontinuous contact problems successfully for future works.

References

Adamus-Bialek, W., Lechowicz, L., Kubiak-Szeligowska, A.B., Wawszczak, M., Kaminska, E. and Charapek, M.A. (2017), "New look at the drug-resistance investigation of uropathogenic E. Coli strains", *Molec. Biol. Report.*, **44**, 191-202. htt://doi.org/10.1007/s11033-017-4099-y.

Aleksendrića, D. and Barton, D.C. (2009), "Neural network prediction of disc brake performance", *Tribol. Int.*, **42**(7), 1074-1080. https://doi.org/10.1016/j.triboint.2009.03.005.

Arani, K.S., Zandi, Y., Pham, B.T., Muazu, M.A., Katebi, J., Mohammadhassani, M., Khalafi, S., Mohamad, E.T., Wakil, K. and Khorami, M. (2019), "Computational optimized finite element modeling of mechanical interaction of concrete with fiber reinforced polymer", *Comput. Concrete*, **23**(1), 61-68. https://doi.org/10.12989/cac.2019.23.1.061.

Ashteyat, A.M. and Ismeik, M. (2018), "Predicting residual compressive strength of self-compacted concrete under various temperatures and relative humidity conditions by artificial neural networks", *Comput. Concrete*, **21**(1), 47-54. https://doi.org/10.12989/cac.2018.21.1.047.

Asteris, P.G., Apostolopoulou, M., Skentou, A.D. and Moropoulou, A. (2019), "Application of artificial neural networks for the prediction of the compressive strength of cement-based mortars", *Comput. Concrete*, **24**(4), 329-345. https://doi.org/10.12989/cac.2019.24.4.329.

Asteris, P.G., Armaghani, D.J., Hatzigeorgiou, G.D., Karayannis, C.G. and Pilakoutas, K. (2019), "Predicting the shear strength of reinforced concrete beams using Artificial Neural Networks", *Comput. Concrete*, **24**(5), 469-488. https://doi.org/10.12989/cac.2019.24.5.469.

Behforouz, B., Memarzadeh, P., Eftekhar, M. and Fathi, F. (2019), "Regression and ANN models for durability and mechanical characteristics of waste ceramic powder high performance sustainable concrete", *Comput. Concrete*, **25**(2), 119-132. https://doi.org/10.12989/cac.2020.25.2.119.

Cakiroglu, E., Comez, I. and Erdol, R. (2005), "Application of artificial neural network to double receding contact problem with a rigid stamp", *Struct. Eng. Mech.*, **21**, 205-220. https://doi.org/10.12989/sem.2005.21.2.205.

Camões, A. and Martins, F.F. (2017), "Compressive strength prediction of CFRP confined concrete using data mining techniques", *Comput. Concrete*, **19**(3), 233-241. https://doi.org/10.12989/cac.2017.19.3.233.

Chandrashekhara, K., Okafor, A.C. and Jiang, Y.P. (1998), "Estimation of contact force on composite plates using impact-induced strain and neural networks", *Compos. Part B-Eng.*, **29**, 363-370. https://doi.org/10.1016/S1359-8368(98)00003-1.

Chitgar, A.G. and Berenjian, J. (2019), "Elman ANNs along with two different sets of inputs for predicting the properties of SCCs", *Comput. Concrete*, **24**(5), 399-412. https://doi.org/10.12989/cac.2019.24.5.399.

Dawson, C.W. and Wilby, R. (1998), "An artificial neural network approach to rainfall-runoff modelling", *Hydrolog. Sci. J.*, **43**(1), 47-66. https://doi.org/10.1080/02626669809492102.

Dehbozorgi, L. and Forokhi, F. (2010), "Effective feature selection for short-term earthquake prediction using Neuro-Fuzzy classifier". *Second IITA International Conference on Geoscience and Remote Sensing*, **2**, 165-169.

Erdem, R.T., Kantar, E., Gücüyen, E. and Anil, Ö. (2013), "Estimation of compression strength of polypropylene fibre reinforced concrete using artificial neural networks", *Comput. Concrete*, **12**(5), 613-625. https://doi.org/10.12989/cac.2013.12.5.613.

Erdogan, F., Gupta, G.D. and Cook, T.S. (1973), "Numerical solution of singular integral equations, in methods of analysis and solution of crack problems", *Noordhoff*, Groningen, Netherlands.

Garzón-Roca, J., Adam, J.M., Sandoval, C. and Roca, P. (2013), "Estimation of the axial behaviour of masonry walls based on artificial neural networks", *Comput. Struct.*, **125**, 145-152. https://doi.org/10.1016/j.compstruc.2013.05.006.

Gazder, U., Al-Amoudi, O.S.B., Khan, S.M.S. and Maslehuddin, M. (2017), "Predicting compressive strength of bended cement concrete with ANNs", *Comput. Concrete*, **20**(6), 627-634. https://doi.org/10.12989/cac.2017.20.6.627.

Hanna, A., Ural, D. and Saygılı, G. (2007), "Evaluation of liquefaction potential of soil deposits using artificial neural networks". *Eng. Comput.*, **24**, 5-16. https://doi.org/10.1108/02644400710718547.

Hasancebi, O. and Dumlupınar, T. (2013), "Linear and nonlinear model updating of reinforced concrete T-beam bridges using artificial neural networks", *Comput. Struct.*, **119**, 1-11. https://doi.org/10.1016/j.compstruc.2012.12.017.

Hattori, G. and Serpa, A.L. (2015), "Contact stiffness estimation in ANSYS using simplified models and artificial neural networks", *Finite Elem. Anal. Des.*, **97**, 43-53. https://doi.org/10.1016/j.finel.2015.01.003.

Hodhod, O.A., Said, T.E. and Ataya, A.M. (2018), "Prediction of creep in concrete using genetic programming hybridized with ANN", *Comput. Concrete*, **21**(5), 513-523. https://doi.org/10.12989/cac.2018.21.5.513.

Kavzoglu, T. (2001), "An investigation of the design and use of feedforward artificial neural networks in the classification of remotely sensed images", PhD Thesis, School of Geography, University of Nottingham

Keskin, R.S.O. and Arslan, G. (2013), "Predicting diagonal cracking strength of RC slender beams without stirrups using ANNs", *Comput. Concrete*, **12**(5), 697-715. https://doi.org/10.12989/cac.2013.12.5.697.

Kong, L., Chen, X. and Du, Y. (2016), "Evaluation of the effect of aggregate on concrete permeability using grey correlation analysis and ANN", *Comput. Concrete*, **17**(5), 613-628. https://doi.org/10.12989/cac.2016.17.5.613.

Krenk, S. (1975), "On quadrate formulas for singular integral-equations of 1st and 2nd kind", *Quart. Appl. Math.*, **33**, 225-232.

Le Cun, Y., Denker, J.S. and Solla, S.A. (1990), "Optimal brain damage", *Adv. Neur. Inform. Proc. Syst.*, **2**, 598-605.

Lin, H.M., Chang, S.K., Wu, J.H. and Juang, C.H. (2009), "Neural network-based model for assessing failure potential of highway

slopes in the Alishan, Taiwan Area: Pre-and post-earthquake investigation", *Eng. Geol.*, **104**(3-4), 280-289. https://doi.org/10.1016/j.enggeo.2008.11.007.

Lingam, A. and Karthikeyan, J. (2007), "Prediction of compressive strength for HPC mixes containing different blends using ANN", *Comput. Concrete*, **13**(5), 581-592. https://doi.org/10.12989/cac.2014.13.5.581.

Mohebbi, A., Shekarchi, M., Mahoutian, M. and Mohebbi, S. (2011), "Modeling the effects of additives on rheological properties of fresh self-consolidating cement paste using artificial neural network", *Comput. Concrete*, **8**(3), 279-292. https://doi.org/10.12989/cac.2011.8.3.279.

Ni, H.G. and Wang, J.Z. (2000), "Prediction of compressive strength of concrete by neural networks", *Cement Concrete Res.*, **30**, 1245-1250. https://doi.org/10.1016/S0008-8846(00)00345-8.

Ongpeng, J., Soberano, M., Oreta, A. and Hirose, S. (2017), "Artificial neural network model using ultrasonic test results to predict compressive stress in concrete", *Comput. Concrete*, **19**(1), 59-68. https://doi.org/10.12989/cac.2017.19.1.059.

Ozsahin, T.S., Birinci, A. and Cakiroglu, A.O. (2004), "Prediction of contact areas between an elastic layer and two elastic circular punches with neural networks", *Struct. Eng. Mech.*, **18**, 441-459. https://doi.org/10.12989/sem.2004.18.4.441.

Ozturk, M., Cansiz, O.F., Sevim, U.K. and Bankir, M.B. (2018), "MLR & ANN approaches for prediction of compressive strength of alkali activated EAFS", *Comput. Concrete*, **21**(5), 559-567. https://doi.org/10.12989/cac.2018.21.5.559.

Rapettoa, M.P., Almqvista, A., Larssona, R. and Lugt, P.M. (2009), "On the influence of surface roughness on real area of contact in normal, dry, friction free, rough contact by using a neural network", *Wear*, **266**(5-6), 592-595. https://doi.org/10.1016/j.wear.2008.04.059.

Saha, P., Prasad, M.L.V and Kumar, P.R. (2017), "Predicting strength of SCC using artificial neural network and multivariable regression analysis", *Comput. Concrete*, **20**(1), 31-38. https://doi.org/10.12989/cac.2017.20.1.031.

Sanad, A. and Saka, M.P. (2001), "Prediction of ultimate smear shear strength of reinforced-concrete deep beams using neural networks", *J. Struct. Eng.*, ASCE, **127**, 818-828. https://doi.org/10.1061/(ASCE)0733-9445(2001)127:7(818).

Serafińska, A., Graf, W. and Kaliske, M. (2018), "Artificial neural networks-based friction law for elastomeric materials applied in finite element sliding contact simulations", *Complexity-Complex Algorithms for Data-Driven Model Learning in Science and Engineering*, 1-15. https://doi.org/10.1155/2018/4396758.

Shebani, A. and Iwnicki, S. (2018), "Prediction of wheel and rail wear under different contact conditions using artificial neural networks", *Wear*, **406-407**, 173-184. https://doi.org/10.1016/j.wear.2018.01.007.

Shirkhania, A., Davarniab, D. and Azar, B.F. (2019), "Prediction of bond strength between concrete and rebar under corrosion using ANN", *Comput. Concrete*, **23**(4), 273-279. https://doi.org/10.12989/cac.2019.23.4.273.

Sipos, T.K., Sigmund, V. and Hadzima-Nyarko, M. (2013), "Earthquake performance of infilled frames using neural networks and experimental database", *Eng. Struct.*, **51**, 113-127. https://doi.org/10.1016/j.engstruct.2012.12.038.

Tang, C.W., Lin, Y. and Kuo, S.F. (2007), "Investigation on correlation between pulse velocity and compressive strength of concrete using ANNs", *Comput. Concrete*, **4**(6), 477-497. https://doi.org/10.12989/cac.2007.4.6.477.

Topcu, I.B., Boga, A.R. and Hocaoglu, F.O. (2009), "Modeling corrosion currents of reinforced concrete using ANN", *Auto. Constr.*, **18**, 145-152. https://doi.org/10.1016/j.autcon.2008.07.004.

Vanluchene, R.D. and Sun, R. (1990), "Neural networks in structural engineering", *Comput. Aid. Civil Infrastr. Eng.*, **5**, 207-215. https://doi.org/10.1111/j.1467-8667.1990.tb00377.x.

Xiaoqiang, R., Wujun, C., Gongyi, F. and Shilin, D. (2005), "Neural network model for solving elastoplastic contact problem", *Chin. J. Appl. Mech.*, 1.

Yan, H., Jiang, Y., Zheng, J., Peng, C. and Li, Q. (2006), "A multilayer perceptron based medical decision support system for heart disease diagnosis", *Exp. Syst. Appl.*, **30**(2), 272-281. https://doi.org/10.1016/j.eswa.2005.07.022.

Yaylacı, M. and Birinci, A. (2013), "The receding contact problem of two elastic layers supported by two elastic quarter plane", *Struct. Eng. Mech.*, **48**, 241-255. https://doi.org/10.12989/sem.2013.48.2.241.

Zurada, J.M. (1992), *Introduction to Artificial Neural Systems*, West Publishing Company, St. Paul.

CC

Appendix 1. Validation patterns

	Input parameters						Desired outputs			
No	$\frac{c}{h_2}$	$\kappa_2 = \kappa_3$	$\frac{a}{h_2}$	$\frac{h_1}{h_2}$	$\frac{\mu_2}{\mu_1}$	$\frac{\mu_3}{\mu_2}$	$\frac{b}{h_2}$	$\frac{(d-c)}{h_2}$	$\frac{P_1^{max}(x)}{P_0}$	$\frac{P_2^{max}(x)}{P_0}$
1	0.01	1.25	0.5	1	2	2	1.2248	1.5307	0.68544	0.50220
2	0.05	1.25	0.5	1	2	2	1.2286	1.4858	0.68298	0.51430
3	0.1	1.25	0.5	1	2	2	1.2341	1.4276	0.67914	0.64447
4	0.5	2	0.1	1	2	2	1.3199	0.9073	0.13846	0.50419
5	0.5	2	0.2	1	2	2	1.3303	0.9148	0.27101	0.99708
6	0.5	2	0.3	1	2	2	1.3473	0.9267	0.39271	1.46863
7	0.5	2	0.5	0.1	2	2	0.5509	0.7248	1.01984	3.42441
8	0.5	2	0.5	0.2	2	2	0.6103	0.7279	1.01980	3.40318
9	0.5	2	0.5	0.3	2	2	0.6796	0.7356	1.01973	3.35071
10	0.5	2	0.5	1	0.25	2	2.2208	1.6374	0.31039	1.16649
11	0.5	2	0.5	1	0.5	2	1.8948	1.3176	0.38425	1.56029
12	0.5	2	0.5	1	0.75	2	1.7324	1.1784	0.44749	1.79972
13	0.5	2	0.5	1	2	1	1.5334	1.1710	0.57186	1.06761
14	0.5	2	0.5	1	2	2	1.4010	0.9652	0.59161	2.31115
15	0.5	2	0.5	1	2	4	1.3296	0.8365	0.60628	3.00229
16	1	1.25	0.5	1	2	2	1.6478	0.4653	0.55918	5.84683
17	1	2	0.5	1	2	2	1.7398	0.4965	0.51467	5.46004
18	1	2.5	0.5	1	2	2	1.7862	0.5169	0.48912	5.23301

Appendix 2. Flow chart of the ANN design